Talanta 109 (2013) 52–60

Contents lists available at SciVerse ScienceDirect

Talanta

journal homepage: www.elsevier.com/locate/talanta

Quantum dots-multiwalled carbon nanotubes nanoconjugate-modified pencil graphite electrode for ultratrace analysis of hemoglobin in dilute human blood samples

Bhim Bali Prasad *, Amrita Prasad, Mahavir Prasad Tiwari

Analytical Division, Department of Chemistry, Faculty of Science, Banaras Hindu University, Varanasi 221 005, India

ARTICLE INFO

Article history:
Received 13 December 2012
Received in revised form
24 January 2013
Accepted 25 January 2013
Available online 4 February 2013

Keywords:
Quantum dots
QDs–MWCNTs nanoconjugate
Hemoglobin
Molecularly imprinted polymer
Real sample analysis

ABSTRACT

A novel molecularly imprinted polymer, selective for human hemoglobin, was immobilized on the surface of CdS quantum dots-multiwalled carbon nanotubes nanoconjugate-modified pencil graphite electrode. The fabricated sensor was found to be water-compatible and biologically benign, since the molecular imprinting was exclusively carried out in water, without any protein denaturation and electrode fouling. Notably, the pencil graphite electrode modified with merely a nanoconjugate matrix might involve the onset possibilities of electrode passivation and protein denaturation. However, a polymer coating onto the nanoconjugate obviated such obstacle while evaluating human hemoglobin in an aqueous environment (pH 4.2). The quantification of the hemoglobin in the dilute whole blood samples varied in the linear range 27.8–444.0 ng mL^{-1}; and the detection limit was obtained as 6.73 ng mL^{-1} ($S/N=3$), without any cross-reactivity and false-positives. The proposed sensor can be used as a cost effective sensor for hemoglobin, in clinical settings.

1. Introduction

Nanoparticulates (NPs) have opened new avenues of molecular recognition. Recently, great efforts have been devoted to the development of nanosensors based on the unique fluorescence emission and optical absorption of nanomaterials for the detections of biological species [1–5]. For example, fluorescent polymer–nanoparticle complexes identify proteins by fluorescence [6]; gold nano-rods or nanoparticles detect peptides [2] and DNA sequences [3] by color changes; hybrid quantum dots (QDs) visualize biomolecules in cells [4]; explosive particulates at surfaces by imaging [5]; and ultra-sensitive visual bioassays of peptide, protein, and DNA using photo luminescent graphene oxide paper like sensors [7]. Successful examples also include the use of QDs as diagnostic tag for protein assays [8–10]. QDs are semiconductor nanoparticles with inherent electronic properties, enormous surface area-to-volume ratio, and specific surface area. Among various NPs, water-soluble QDs have shown great potential because of their unique advantages: nanoscale size similar to proteins, broad excitation spectra for multicolor imaging, robust, narrow band emission, and versatility in surface modification [11–13]. Currently, the development of practical strategies for assembling QDs onto carbon nanotubes (CNTs) surface is an area of considerable interest. Hetero-junction of QDs and CNTs could render a better platform for nanoscale sensing [14–16] as compared to QDs and multi-walled carbon nanotubes (MWCNTs) used alone [17,18]. Inspired by this, for the first time, we have synthesized a molecularly imprinted polymer (MIP)-based electrochemical sensing system for human hemoglobin (Hb) at the surface of QDs–MWCNTs nanoconjugate.

Molecular imprinting technique is based on the development of a non-covalent complex using the target (template) molecules and suitable functional monomer(s). Subsequently, a cross-linker, say ethylene glycol dimethacrylate, is added to this mixture to form a matrix in which the complexes are fixed. After template extraction from this mixture, a tailor made highly selective synthetic receptor is created which can rebind the analyte according to its shape and functionality. Although, molecularly imprinted polymer (MIP)-based sensors using optical properties of QDs have widely been explored [19–25], MIP-based electrochemical sensing using QDs is extremely rare [26]. Notably, MIP-based electrochemical sensor at the surface of QDs–MWCNTs nanoconjugate has not yet been reported. Surface

Abbreviations: NPs, nanoparticulates; QDs, quantum dots; AC, acryloyl chloride; CNTs, carbon nanotubes; MWCNTs, multi-walled carbon nanotubes; Hb, hemoglobin; MIP, molecularly imprinted polymer; L-Cys, L-Cystein; PGE, pencil graphite electrode; AC, acryloyl chloride; PBS, phosphate buffer solution; TDW, triple distilled water; NMGA, N-methacryloyl glutamic acid; DAU, diacryl urea; SDS, sodium dodecyl sulfate; SDTC, sodium N, N-diethyldithiocarbamate; DPCSV, differential pulse cathodic stripping voltammetry; CV, cyclic voltammetry; SEM, scanning electron microscope; TEM, tunneling electron microscopy; NIP, non imprinted polymer; RSD, relative standard deviation; LOD, limit of detection; AA, ascorbic acid; Crp, C-reactive protein; Dop, dopamine; Glu, glutamic acid; Ins, insulin; HPLC, high performance liquid chromatography

* Corresponding author. Tel.: +91 9451954449.
E-mail address: prof.bbpd@yahoo.com (B.B. Prasad).

0039-9140/$ - see front matter © 2013 Elsevier B.V. All rights reserved.
http://dx.doi.org/10.1016/j.talanta.2013.01.051

imprinting at nanoconjugate would facilitate the complete template removal and provides better site accessibility, lower mass transfer resistance, and well-defined material shape, in contrast to the traditional bulk imprinting approach [27]. In this work, we have first synthesized the CdS–QDs–MWCNTs nanoconjugate by covalent attachment of L-Cystein (L-Cys) capped CdS onto the MWCNTs–COCl pre-cast on a pencil graphite electrode (PGE). The remaining carboxylic groups on the surface of CdS-QDs were used to attach an iniferter (initiator-transfer terminating agent) group which resulted in the development of a controlled surface-grafted imprinted polymer. The choice of functional monomer, cross linker, and CdS-QDs–MWCNTs nanoconjugate was based on the fact that all were water-soluble and hence biocompatible (ignoring negligible toxicity due to very small amounts of CdS over the tip of electrode) for protein imprinting, in aqueous medium [for details on CdS-QDs and MWCNTs, vide Supporting Information in Section S1].

Increasing importance of protein recognition in proteome study has triggered the development of highly selective and efficient analytical methods since proteins are central in understanding most diseases. The target analyte, Hb, is a typical heme protein that functions physiologically in the storage and transport of molecular oxygen in mammalian blood and manifests many chronic diseases. Compared with traditional spectroscopic method, electrochemical technique is most preferred method of the determination of Hb because it can overcome the major disadvantages in terms of requiring toxic reagents, time-consuming sample pretreatment, and greater influence of pigments and turbidity associated with the spectroscopic measurement [28,29]. Nevertheless, the large three-dimensional structure of heme protein, the resulting inaccessibility of the heme center, and the subsequent electrode passivation due to protein adsorption have posed critical problems in obtaining direct electron transfer between protein and conventional electrodes [30]. Sincere efforts have been made to improve electron-transfer by using mediators, promoters or some special modifying materials including biopolymers, self-assembled monolayers, metal (oxide) nanoparticles, etc. [31–34]. However, only a few methods have been reported dealing electroanalysis of Hb in blood and that too with higher detection limit and poor selectivity [32–34]. Moreover, in another seminal work [33] the sensitivity of electrochemical measurement in blood was not improved even a complicated flow injection analysis system was coupled with electrochemical transduction. Although several MIPs have been developed for Hb without revealing analytical aspects [35–38], they are not exploited for sensor fabrication. The major bottleneck in Hb analysis is sensor fouling due to an irreversible adsorption of protein on the electrode surface. To prevent adsorption of protein on the sensor surface, a hydrophilic and polar MIP is required. Furthermore, the whole blood samples have to be diluted enough to mitigate the effect of complicated matrices. However, such dilutions lower detection limits and, therefore, a highly selective and sensitive method of analysis is called for.

2. Experimental section

2.1. Materials and reagents

All chemicals were of analytical reagent grade, and used without further purification. Acryloyl chloride (AC), methacryloyl chloride, urea, sodium N, N-diethyldithiocarbamate (SDTC), and L-Cys, were purchased from Loba chemie (Mumbai, India) and Spectrochem Pvt. Ltd. (Mumbai, India). Chloroacetyl chloride, MWCNTs (internal diameter 2–6 nm, outer diameter 10–15 nm, length 0.2–10 μm, and purity > 90%), sodium dodecyl sulfate (SDS), Hb and its interferents, were purchased from Aldrich (Steinheim, Germany) and Fluka (Steinheim, Germany). Tris buffer and cadmium chloride were obtained from Hi media laboratories and Qualigens fine chemicals (Mumbai, India). Phosphate buffer solution (PBS) (pH 4.2, ionic strength 0.1 M), was used as a supporting electrolyte. Standard stock solution of Hb (500.0 μg mL^{-1}) was prepared daily using deionized triple distilled water (TDW) (conducting range $0.06–0.07 \times 10^{-6}$ S cm^{-1}). All working solutions were prepared by diluting stock solution with water. The pH values of test solutions were adjusted by the addition of a few drops of either 0.1 M HCl or 0.1 M NaOH. Human blood samples were obtained from the Institute of Medical Sciences, Banaras Hindu University (Varanasi, India), and used without any sample pretreatment. All blood samples were kept in a refrigerator at ~4 °C, before use. The water-soluble L-Cys capped CdS QDs were synthesized according to a known procedure [39]. Monomeric precursor, N-methacryloyl glutamic acid (NMGA) was synthesized and characterized following a known recipe [40]. Synthesis and characterization of water-soluble cross-linker, diacryl urea (DAU), are described elsewhere [41]. The details on the preparation of these materials are provided in the Supporting Information (Sections S2–S4).

2.2. Apparatus

Differential pulse cathodic stripping voltammetry (DPCSV), chronocoulometry, and cyclic voltammetry (CV), were performed using a three electrode cell assembly consisted of MIP-modified PGEs, platinum wire, and Ag/AgCl (saturated KCl) as working, counter, and reference electrodes, respectively. Voltammetric measurements were carried out with a polarographic analyzer / stripping voltammometer [model 264A, EG & G Princeton Applied Research (PAR), USA] in conjunction with an electrode assembly [PAR model 303A] and an *X–Y* chart recorder (PAR model, RE 0089). Chronocoulometry measurements were performed with an electrochemical analyzer (CH instruments, USA, model 1200A). FT-IR (KBr) was recorded on Varian FT/IR (USA) spectrometers. Morphological images of bare and modified electrode surfaces were obtained using a scanning electron microscope (SEM), [JEOL model, JSM-6390 LV (USA)] and a tunneling electron microscope (TEM, Phillips EMCM-12 model). UV–visible spectra were recorded on a Varian Cary 100 Bio UV–visible spectrophotometer (USA).

2.3. Sensor fabrication

First, a pencil rod (2B) was pretreated by dipping in 6 M HNO_3 for 15 min, washing with water, and subsequently smoothening the surface by soft cotton. This was inserted into a Teflon tube, where the tip of the pencil rod at one end was gently rubbed, with an emery paper (No. 400), to level the pencil surface along the tube orifice. Electrical contact was obtained by soldering a metallic wire to the exposed reverse side of the pencil rod. The use of PGE in lieu of noble metal electrodes (Au, Ag, Pt, Pd etc.) is advantageous in terms of its cost effectiveness, wider potential window, and relatively less background current [42].

The Hb imprinted QDs–MWCNTs nanoconjugate-modified PGE sensor (MIP–Hb/QDs–MWCNTs/PGE), was developed following three steps (Scheme 1A and B):

1. *Attachment of QDs–MWCNTs nanoconjugate to PGE surface*: PGE was spin coated with functionalized MWCNTs as MWCNT–COCl (15 mg in 1 mL water) at 2600 rpm for 30 s. The functionalization of MWCNTs was necessary to inculcate water compatibility in CNTs. For this, MWCNTs were first

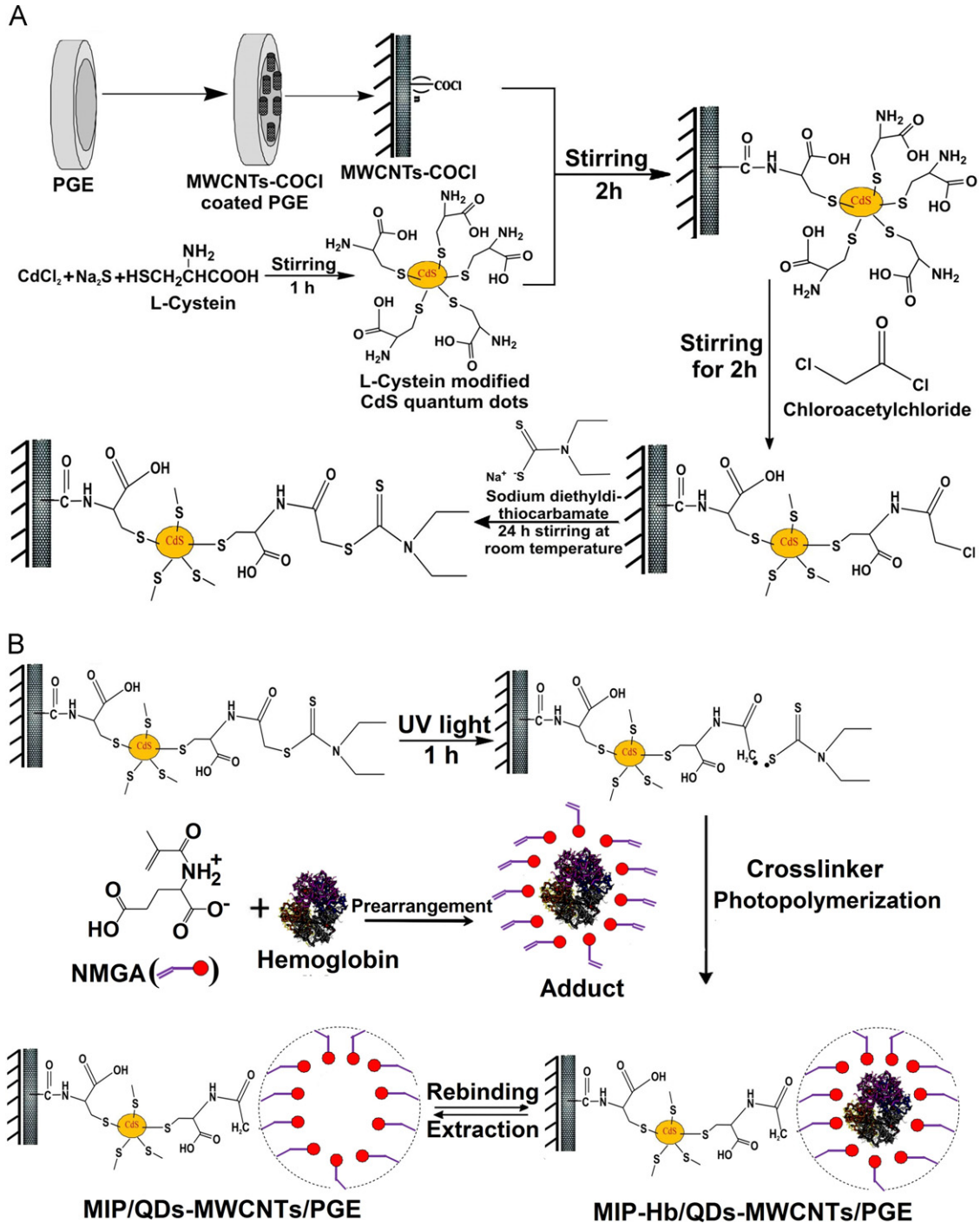

Scheme 1. (A) Schematic representation showing immobilization of iniferter on QDs-MWCNTs nanoconjugate-modified PGE. (B) Fabrication of MIP-modified QDs-MWCNTs/PGE.

subjected to acid treatment to obtain MWCNTs–COOH and then reacted with $SOCl_2$ to convert as MWCNT–COCl [43]. During spin coating of MWCNTs–COCl, MWCNTs were physically adsorbed to the PGE surface, via their penetration into graphite micro-pores. This way MWCNTs remained intact at PGE surface and these could not be washed away when the surface is immersed in the QDs solution (10 mg in 500 μL water) for 2 h with continuous stirring. This helped forming amide bonds between MWCNTs–COCl and NH_2 group of QDs to yield QDs–MWCNTs nanoconjugate.

2. *Immobilization of iniferter at QDs–MWCNTs/PGE*: QDs–MWCNTs nanoconjugate modified PGEs were treated with chloroacetyl chloride under stirring for 2 h. Subsequently, these electrodes were treated with SDTC (0.1 M) and kept for 24 h, under stirring at room temperature.
3. *Surface imprinting*: The iniferter modified QDs–MWCNTs/PGE was first irradiated in UV light (Philips UV lamp delivering 9 W cm^{-2}) for 1 h with intermittent exposure at 10 min intervals. The prepolymerization reaction mixture [template (Hb, 0.007 mmol/1.0 mL tris buffer), monomer (NMGA, 0.014 mmoL/1.0 mL water), and crosslinker (DAU, 0.14 mmoL/1.0 mL water)] was mixed together and the whole content was purged with N_2 gas for 10 min. Latter, this mixture (10.0 μL) was spin-coated onto the iniferter-modified QDs–MWCNTs/PGE, at 2600 rpm for

30 s, followed by re-irradiation with UV lamp for 3 h with intermittent exposure at 10 min intervals to initiate radical polymerization. After photo-polymerization, a MIP-template adduct layer on the surface of QDs–MWCNTs/PGE was formed (Scheme 1B). The similar procedure was adopted to prepare the non-imprinted polymer (NIP)-grafted QDs–MWCNTs/PGE, in the absence of template (Hb). Finally, all template molecules were retrieved from the water-insoluble polymeric (MIP-template adduct) film by immersing the modified electrode into SDS:acetic acid (1:2, v/v, 10% each) mixture for 60 min. This yielded a hydrophilic and polar surface of MIP layer. The complete template removal was confirmed, until no voltammetric response of the template was observed.

2.4. Electroanalytical measurement

MIP-modified PGE (working electrode) was brought into the voltammetric cell containing 10.0 mL PBS (pH 4.2, ionic strength 0.1 M) to record blank run. The freshly prepared Hb solution was introduced into the cell and allowed the analyte accumulation, at an optimized potential (E_{acc}) of 1.0 V, for accumulation time (t_{acc}) 60 s under dynamic condition. The CV curves were recorded under cathodic stripping mode from +0.7 to −0.6 V, respective to Ag/AgCl, at different scan rates of 10–200 mV s^{-1}. DPCSV runs were obtained at 10 mV s^{-1}, with 25 mV pulse amplitude. Since dissolved oxygen present in the cell did not affect stripping current, de-aeration of the cell content was not necessary. All experiments were carried out at room temperature (25 ± 1 °C). Voltammetric measurements were also performed with the NIP electrode, under identical operating conditions as mentioned above.

3. Results and discussion

3.1. UV–visible absorption studies

UV–visible spectroscopy is an important tool to examine the conformational integrity of heme proteins. The possible denaturation of heme proteins can be indicated by the position of the Soret absorption band of iron heme. When Hb is denatured, its Soret band would either shift or disappear. Fig. S1 in Supporting Information shows UV visible spectra of Hb dissolved in Tris buffer solution (pH=6.8, curve A), Hb/Tris buffer solution in supporting electrolyte PBS (pH 4.2, curve B), Hb-nujol paste casted on Whatmann filter paper (curve C), and MIP–Hb adduct (modified on QDs–MWCNTs nanoconjugate in the form of nujol paste) casted on Whatmann filter paper (curve D). Accordingly, Hb solution in tris buffer has showed a Soret band at 408 nm (curve A) and the dry cast Hb film on filter paper responded an absorption band at 410 nm (curve C). Interestingly, the Hb Soret band appeared almost at the same position at 408 nm in the medium PBS (curve B) and at 412 nm when casted with MIP (curve D). Thus the position of Soret absorption bands shifted maximally to 4 nm that is almost insignificant to indicate any Hb denaturation. This suggests that Hb retains its native conformation both in working solution (PBS, pH 4.2) as well as in the texture of MIP modified at QDs–MWCNTs nanoconjugate surface. That means MIP/QDs–MWCNTs has offered a "near aqueous environment" to Hb molecules so as to retain protein conformation and biological activity, without any deterioration.

3.2. Polymer characteristics

As a consequence of the complexity of structure, sequence variations, folding motifs and surface adsorption characteristics of protein, a high level of specificity in protein recognition is required. This can only be achieved by synthesizing a MIP prepared through the three-dimensional distribution of functional groups and by the introduction of a large number of weak complementary interactions in aqueous environment. In this work, it could be maneuvered through the electrostatically driven self-assembling of the functional monomer(s) around a template molecule in an ordered low-energy configuration, followed by the polymerization in aqueous condition leading to the formation of a water-compatible MIP [44,45]. The hydrophilic and polar MIP network so produced has ability to bind larger template on the basis of shape complementarity and multipoint weak electrostatic and hydrogen bondings. However, there could be restricted mobility of large molecule within highly cross-linked polymer network resulting in poor reversibility and efficiency in binding. Apparently, the surface grafting might be considered as a most viable way to resolve this situation. In this work, template-monomer molar ratios were systematically varied (1:100, 1:150, 1:200, 1:250, and 1:300) in order to explore an optimized complex that can lead to the maximum development of the current response. The optimized template-monomer ratio in the present instance was 1:200; the less monomer content might not have the required ability to withhold template molecules, whereas the higher amount of monomer caused heterogeneity in binding sites and thereby a low current response. Insofar as the cross-linker amount is concerned, as much as 0.14 mmol DAU in the presence of 0.007 mmol Hb and 1.4 mmol NMGA (template: cross-linker ratio 1: 20) was found to be an optimum composition to give rise to maximum DPCSV current response. Notably, in this work, any cross-linker amount taken more than 0.14 mmol have rendered stiffness to the polymer network that severely restricted the analyte access to molecular cavities. Furthermore, the template molecules exceeding 0.007 mmol might lead to an incomplete pre-organization of functional groups, and hence the diminishing binding sites of high performance. Controlling the amount of Hb molecules to locate entirely on the surface of imprinted material is actually required to obtain homogenous binding sites, without any template aggregation and/or denaturation in the imprinting solvent (porogen).

Another factor which appeared to be crucial in this work was the effect of loading of MWCNTs–COCl on the surface of sensor. The maximum current response was obtained when optimum amount of 15 mg MWCNTs–COCl was loaded on the surface. Any amount higher than this always revealed agglutination and poor dispersibility of MWCNTs–COCl in the coating. As far as the spin time and speed, which affect the thickness of MIP film, were concerned, a maximum spin time of 30 s at 2600 rpm was required to develop a highly responsive MIP film of optimum thickness using 15.0 μL of pre-polymer mixture (vide Section 3.4). Other polymerization conditions (e.g., polymerization time and polymerization temperature) govern the extent of porosity in the polymer texture. Given short duration for the polymerization (< 3 h), binding sites were appeared to be inadequate to respond maximum development of the current. On the other hand, the longer polymerization time (> 3 h) might lead to an extensive cross-linking, and thereby the higher thickness with restricted porosity in the film. This might also render the poor site accessibility of imprinted cavities to protein encapsulation. Thus, the polymerization time of 3 h was optimum to obtain the maximum current response. Insofar as polymerization temperature is concerned, a moderate temperature of 37 °C was found appropriate to respond optimum current; any temperature below this may cause a sluggish polymerization and take longer time.

3.3. Spectral and morphological characterizations

FT-IR (KBr) spectra of scrapped coating (~5 mg collected from bunch of electrodes), before and after iniferter modification at QDs–MWCNTs/PGE surface (Scheme 1A), are shown in Fig. S2 in Supporting Information. The proposed binding mechanism

(Fig. S3, Supporting Information) was supported by FT-IR (KBr) spectra of monomer (NMGA), template (Hb), MIP-adduct, and MIP (Fig. S4, Supporting Information). For details on spectral characterizations, vide Supporting Information (Section S5). As evinced from Fig. S3, the coating material was obviously a polar substance that possessed hydrophilic characteristics to prevent adsorption of protein on the modified PGE surface.

Surface morphologies of each layer at PGE are shown in SEM images (Fig. 1). MWCNTs–COCl/PGE could be visualized as interconnected nanotubes (Fig. 1A). Fig. 1B shows QDs–MWCNTs nanoconjugate-modified PGEs surface, where some distinctly visible CdS nanoparticles appear to enhance the thickness of nanotubes. Herein, QDs could be spotted one by one onto the sidewalls of MWCNTs–COCl, manifesting the highly conjugated QDs-MWCNTs heterojunctions. Apparently, MIP–Hb-adduct/QDs–MWCNTs/PGE is compact (Fig. 1C) as compared to MIP/QDs–MWCNTs/PGE surface (Fig. 1D). The latter carrying exposed cavities could easily be accessible for Hb rebinding. The SEM side image of the MIP/QDs–MWCNTs/PGE (Fig. S5, Supporting Information) revealed the coating thickness to be 61 nm, which was obtained under optimized parameters of spin-coating method.

TEM images of CdS nanoparticles and QDs–MWCNTs are shown in Fig. 1(E) and (F). Accordingly, the TEM image for a few focused QDs revealed an average particle size of about 15 nm with narrow size variation (Fig. 1E). However, the respective image (Fig. 1F) of QDs–MWCNTs nanoconjugate did not reveal any QDs aggregation. This suggests homogeneously dispersed QDs all along MWCNTs, in the nanoconjugate.

3.4. Binding affinity

Affinity constant of Hb serving as template can be estimated on the basis of Langmuir adsorption isotherm. Accordingly, the affinity constant i.e, adsorption equilibrium constant and corresponding Gibbs free energy change due to analyte adsorption onto MIP film were obtained as 4.69×10^{8} L mol^{-1} and -59.42 KJ mol^{-1}, respectively [For details vide Supporting Information Section S6].

The binding capacity of any MIP is primarily dependent upon the thickness of the film coated on electrode [46]. An optimizing form of imprinted material should have small dimension with a high surface-to-volume ratio, which can simply facilitate the template removal, improve the surface accessibility to the target analyte, and reduce the mass-transfer resistance. In this context, we have explored the interrelation between the effectiveness of film immobilization conditions (i.e, spin time and speed) and the binding amount (i.e, proportional to the magnitude of binding signal). Fig. S6(A) and (B) shows the evolution of DPCSV current with decrease of film thickness, consequent upon the increase of spin time/speed. With increase of spin coating conditions (time and speed), the DPCSV current for Hb (108.2 ng mL^{-1}) increased and reached the maximum when an optimum film thickness (61 nm) was developed at the PGE surface applying the spin time of 30 s and at spin rate of 2600 rpm. The further increase of spin time or speed did not lead to a stable coating owing to the formation of an ultrathin coating with limited binding cavities; and thereby, a decline in current was observed. This suggests that 61 nm (Fig. S5) may be considered as a critical thickness of MIP film to offer better site accessibility to target molecules with maximum binding capacity.

3.5. Electrochemical characteristics of QDs–MWCNTs nanoconjugate layer

The effect of QDs–MWCNTs nanoconjugate layer at PGE was studied voltammetrically using 0.01 M $Fe(CN)_6^{3-}$/ $Fe(CN)_6^{4-}$ probe at bare, QDs, MWCNTs, and QDs–MWCNTs nanoconjugate-modified PGEs (Fig. 2A). This shows corresponding CV reversible peaks at bare PGE (run 1). At QDs/PGE these peaks are consistent in terms of peak height with the bare PGE indicating literally no alternation in peak current on QDs coating at PGE (run 2). On the other hand, simply coating MWCNTs on PGE, the respective current was found to be increased substantially (run 3) with cathodic-anodic peak current ratio (I_{pc}/I_{pa}) of 0.7 and peak separation (ΔE_p=90 mV). However, such peaks for $Fe(CN)_6^{3-}$ probe are relatively amplified assuming a

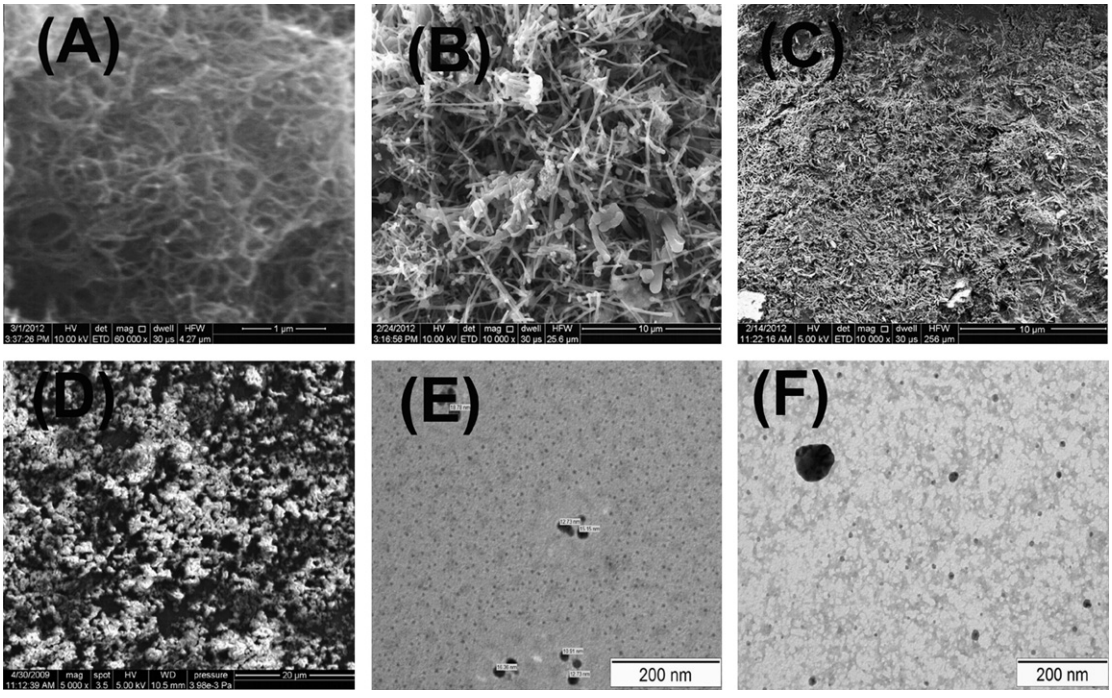

Fig. 1. SEM images: (A) MWCNTs–COCl/PGE, (B) QDs–MWCNTs/PGE, (C) MIP–Hb/QDs–MWCNTs/PGE, and (D) MIP/QDs–MWCNTs/PGE. TEM image: (E) QDs and (F) QDs–MWCNTs nanoconjugate.

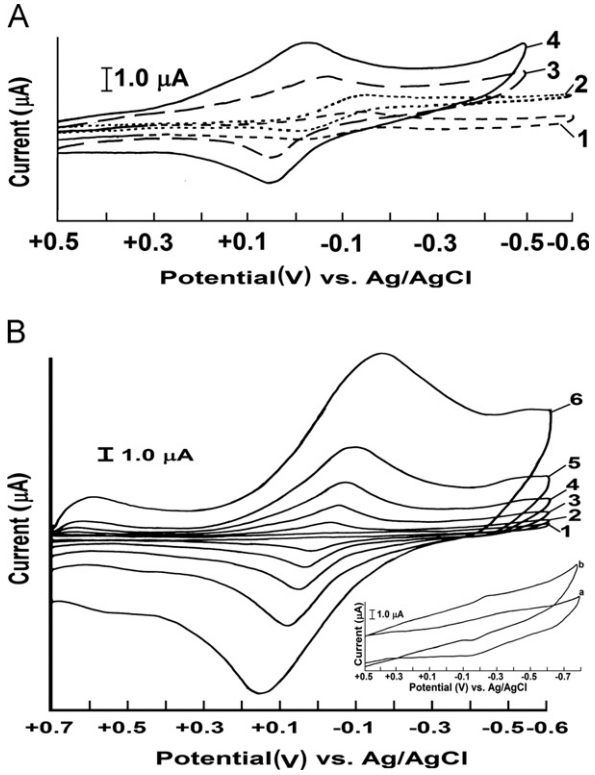

Fig. 2. (A) CV response for $[Fe(CN)_6]^{3-/4-}$ (0.01 M) probe at (1) bare PGE, (2) QDs/PGE, (3) MWCNTs/PGE, and (4) QDs–MWCNTs/PGE at scan rate 10 mVs^{-1}. (B) CV runs in cathodic stripping mode with MIP/QDs-MWCNTs/PGE: blank run in the absence of Hb (10 mVs^{-1}, run 1) and runs 2–6 at different scan rates 10–200 mVs^{-1}, for 24.87 ng mL^{-1} Hb (Inset represents CV on bare PGE (run a) and QDs-MWCNTs/PGE (run b) for Hb concentrations 499.05 and 24.87 ng mL^{-1}, at scan rate 10 mVs^{-1}).

highly symmetrical characteristics when a combination of QDs and MWCNTs was used for the modification. The ΔE_p (~60 mV) and I_{pc}/I_{pa} ratio (1.0) with run 4 revealed a perfect reversible behavior of QDs–MWCNTs modified PGE. One may presume some sort of coordinated interactions and/or some synergistic effect between QDs and MWCNTs that helped upbringing an improved catalytic action toward the electrodics of modified electrode. The electrocatalytic action in this case could be evident from the fact that a relatively less energy was required for the cathodic stripping since reduction potential shifted positively on QDs–MWCNTs nanoconjugate-modified PGE in comparison to the QDs- or MWCNTs-modified PGEs (cf, runs 2–4).

3.6. Electrochemical behavior of Hb

Electrochemical behavior of Hb (24.9 ng mL^{-1}) was investigated by CV (cathodic stripping mode) at different scan rates using MIP/QDs–MWCNTs/PGE (Fig. 2B). The bare and QDs–MWCNTs/PGE were also explored to obtain CV runs for 499.0 and 24.9 ng mL^{-1} Hb, respectively (Fig. 2B, inset). In all cases, the test analyte was first accumulated at +1.0 V (E_{acc}) for accumulation time (t_{acc}) 60 s, allowed to attain an equilibrium for additional 15 s, and then subjected to cathodic stripping. This resulted in a cathodic peak in forward scan followed by an anodic peak on reverse scan. The electron-transfer process can be described as follows [47]:

$$\text{Hb heme Fe (III)} + H^+ + e^- \rightleftharpoons \text{Hb heme Fe (II)} \quad (1)$$

The bare electrode showed ill-defined electrochemical behavior even for Hb concentration taken as high as 499.0 ng mL^{-1}. The CV run on QDs–MWCNTs/PGE for Hb (24.9 ng mL^{-1}) did not reveal any distinctive improvement upon modification. However, for this concentration of Hb, CV peaks are found to be highly improved and symmetrical on MIP/QDs–MWCNTs/PGE at scan rates of 10–200 mV s^{-1}. The peak separation (ΔE_p) realized at 10 mV s^{-1} with this electrode indicates the reversible behavior of electron-transfer process; nevertheless this turned to behave pseudo-reversible (ΔE_p, 80–200 mV) with increasing scan rates (20–200 mV s^{-1}). The quasi-reversibility trends may be attributed to the blocking effect toward electron-transfer on reverse scan. The blocking occurred due to the electrode surface coverage of the reduced product, which could not be retrieved easily within the limited time span of oxidation at higher scan rates. Thereby, the more energy was required for anodic oxidation causing a moderate anodic shift ($\leq$20 mV) of oxidation peak potential. On the other hand, the similar order of cathodic shift of reduction peak in the forward scan might be accorded with the strong occupation of Hb oxidized [i.e., Hb heme Fe (III) at E_{acc}+1.0 V] molecules in molecular cavities that consumed a bit more energy for stripping in cathodic mode. The broad peak widths at all scan rates support the strong adsorption of both reduced and oxidized species; pre- and post-adsorption peaks are appeared at extreme ends of voltammograms (pre- and post-adsorption peaks could be seen more vivid at high scan rates). Furthermore, the both reduction and oxidation peak currents (I_{pc} and I_{pa}) increased linearly with the scan rates as follows:

$$I_{pc} = (-2.000 \pm 0.952) + (0.731 \pm 0.109)v^{1/2} \quad (2)$$

$$I_{pa} = (-2.070 \pm 0.628) + (0.815 \pm 0.072)v^{1/2} \quad (3)$$

The linearity of the I_{pc} or I_{pa} with scan rate suggests that the electrode reaction is a diffusion controlled process at the surface of MIP/QDs–MWCNTs/PGE. The electron transfer rate constant (K_s) could be obtained according to Laviron's equation [48]: $K_s = mnFv/RT$, where m is a parameter related to peak to peak separation (the dependence of $n\Delta E_p$ as a function of 1/m for α=0.5 can be referred to an earlier work [48]), F the Faraday constant, v the scan rate (V s^{-1}), R the gas constant, T the temperature, and n is the number of electron transfer. Assuming that electron transfer coefficient (α) is not too different from 0.5 and electrode process is quasi-reversible, K_s values of the bare PGE, QDs–MWCNTs/PGE, and MIP/QDs–MWCNTs/PGE are calculated as 0.029 ± 0.004, 0.111 ± 0.002 and 0.315 ± 0.002 s^{-1}, respectively. The higher K_s value on MIP-modified PGE as compared to bare PGE and QDs–MWCNTs/PGE reflects that the QDs nanoparticles increase the surface area, active point for adsorbing Hb, and also make the film more porous to facilitate electron transfer.

Differential pulse modulation amplitude as much as 25 mV and pulse width of 50 ms in DPCSV afforded a high level of sensitivity in the sufficient time scale in comparison with CV, at optimized operating conditions. Fig. 3A displays DPCSV currents in the absence of analyte on bare, QDs–MWCNTs/PGE, and MIP/QDs–MWCNTs/PGE represented by columns 2, 5, and 8, respectively. These electrodes were then subjected to DPCSV measurements for different concentrations of aqueous solution of Hb (Fig. 3A). Like CV, the unmodified (bare) electrode was found insensitive to quantify Hb concentrations lower than 499.0 ng mL^{-1} (column 3). However, upon modification as QDs–MWCNTs/PGE the sensitivity of DPCSV measurement, unlike CV, was slightly improved so that this electrode could able to respond (column 6), even at lower Hb concentration (24.9 ng mL^{-1}). Nevertheless, both DPCSV measurements (columns 3 and 6) were found not to be quantifiable, as revealed by disproportionate current heights (columns 4 and 7), obtained by the method of standard addition. This could be attributed to the electrode blocking and thereby passivation on account of intensive irreversible adsorption of protein molecules at the active surface of the modified

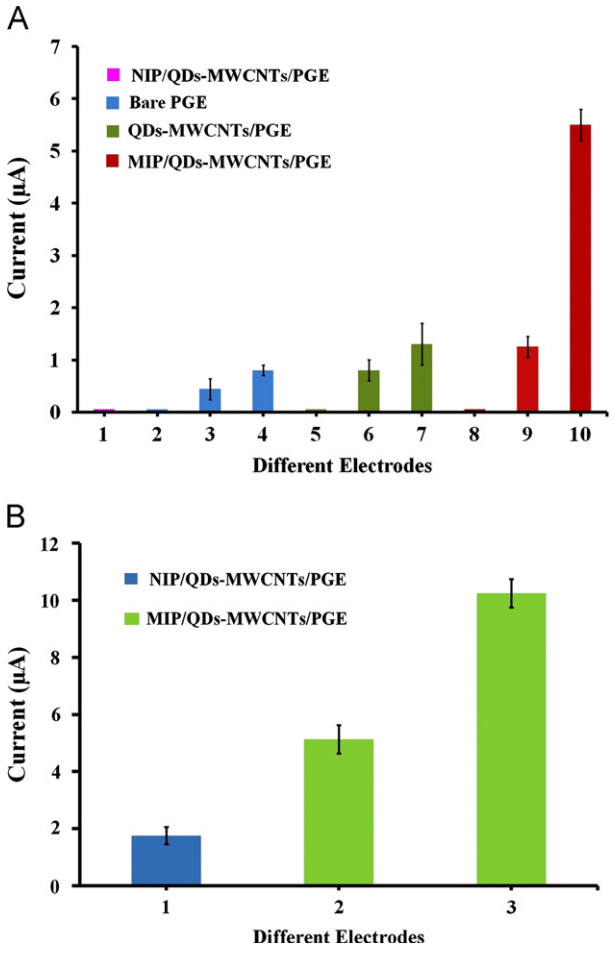

Fig. 3. (A) DPCSV measurements on different electrodes in absence of Hb (columns 2, 5, 8) and at different concentrations (ng mL^{-1}) of aqueous solutions of Hb (column 1) 108.02, (column 3) 499.05, (column 4) 745.80, (column 6) 24.87, (column 7) 108.02, (column 9) 24.87, (column 10) 108.02. (B) DPCSV measurements NIP- and MIP-modified sensors for different concentrations (ng mL^{-1}) of Hb in human blood samples (column 1) 108.02, (column 2) 101.83, (column 3) 199.83.

electrode [35]. Furthermore, the electron transfer of Hb was very slow to respond any quantifiable current at conventional electrodes. The surfaces of the unmodified electrode were incompetent to restrict protein denaturation, upon Hb rebinding. These attendant problems can easily be resolved by modifying electrodes with mediators or promoters or incorporating enzymes and proteins into various films immobilized on the electrode surface [31]. In this work, MIP modification was found to be advantageous not only to resolve the aforesaid problems but also to respond the quantitative recovery with specific recognition. As a matter of fact, the same Hb concentration of 24.9 ng mL^{-1} was specifically recognized (column 9) and quantified by spiking (column 10) on MIP/QDs–MWCNTs/PGE. Fortuitously, the corresponding NIP-modified electrode did not respond any non-specific adsorption (column 1), irrespective of analyte concentration. The proposed MIP-modified electrode responded following linear calibration equation between DPCSV peak current (I_p, μA) and analyte concentration (C, ng mL^{-1}) for aqueous solutions of Hb, with the limit of detection (*LOD*, computed as 3σ by the standard procedure [49]) and analyte recovery (optimized operating conditions: E_{acc} 1.0 V, t_{acc} 60 s, pH 4.2; for details regarding optimization of analytical parameters vide Supporting Information Section S7).

For Hb concentration range 24.9–454.7 ng mL^{-1}, $I_p=(0.048\pm0.001)\ C+(0.196\pm0.129)$, $R^2=0.999$, $n=8$. $LOD=7.08$ ng mL^{-1} [3σ, relative standard deviation (RSD)=1.06%], recovery=98.7–101.7%.

3.7. Chronocoulometry

Electro-reduction of Hb at the MIP/QDs–MWCNTs/PGE was also characterized by chronocoulometry. In this study, the Anson plot of charge against square root of time ($Q-t^{1/2}$) showed a linear relationship in the presence of Hb. From the slope of this plot, diffusion coefficient (D) is obtained as 2.2×10^{-6} $cm^2\ s^{-1}$. The surface coverage concentration (Γ^0) of analyte molecules, which were specifically bound to MIP cavities (electrochemically accessible) over the modified surface of the electrode (electrochemical surface area 0.232 cm^2) is calculated as 1.16×10^{-10} mol cm^{-2} [For details on chronocoulometry, vide Supporting Information Section S8].

3.8. Analytical applications

The real applications of the proposed MIP/QDs–MWCNTs/PGE sensor were explored for Hb determination in whole human blood samples (diluted 10^5-fold). The linear calibration equation between DPCSV peak current (I_p, μA) and Hb concentration (C, ng mL^{-1}) was realized as

For Hb concentration range 27.8–444.0 ng mL^{-1}, $I_p=(0.050\pm0.000)\ C+(0.009\pm0.026)$, $R^2=0.999$, $n=8$. $LOD=6.73$ ng mL^{-1} (3σ, $RSD=1.02\%$), recovery=98.4–100.0%.

DPCSV peaks in highly diluted blood samples are found highly symmetrical like those obtained with aqueous samples. Various blood samples of different patients were also studied for the validation of the proposed sensor (Table 1). The DPCSV measurements on NIP-(columns 1) and MIP- modified QDs–MWCNTs/PGE (columns 2 and 3) at different analyte concentrations are shown in Fig. 3B. The Hb concentration range in normal blood serum is known to be 10–13 g dL^{-1} [50]. Under this situation, the blood samples have to be diluted as many as 10^5 fold so as to move the detection within the range of detection limits of the sensor and also to mitigate the matrix effect to the larger extent. Any pretreatment such as deproteinization and/or ultrafiltration has deliberately been avoided as this may lead inaccuracies in the final results. Instead, the dilution was found to be very effective against matrix effect since the sample behavior almost

Table 1
Analytical results of DPCSV measurements on MIP/QDs–MWCNTs/PGE for Hb in whole blood samples of different patients.

Sample	Analyte (Hb) concentration (ng mL^{-1})	Hb concentration determined (ng mL^{-1})	Recovery (%)	*RSD* (3σ)	Hb concentration[a] obtained from the present technique (g dL^{-1})
Patient 1	Unknown	232.0 ± 2.6	–	–	11.62 (12.00)
	308.37	308.2 ± 3.0	99.9	0.97	
	352.77	346.9 ± 2.6	98.3	0.75	
Patient 2	Unknown	236.9 ± 3.2	–	–	11.87 (12.30)
	311.23	318.0 ± 2.0	102.1	0.62	
Patient 3	Unknown	193.6 ± 2.0	–	–	9.69 (10.30)
	302.2	294.7 ± 3.5	97.5	1.18	
Patient 4	Unknown	256.9 ± 4.9	–	–	12.87 (13.60)
	301.59	297.9 ± 2.1	98.8	0.71	

[a] Hb concentration in whole blood obtained by multiplying Hb concentration measured in diluted blood samples with a dilution factor of 5.01×10^5. The concentrations in parentheses are certified values measured using the conventional spectrophotometric method in pathology laboratory.

Table 2
Comparison of different methods for Hb detection.

S.N	Method	Sensitivity (ng mL^{-1})	Range (ng mL^{-1})	Recovery (%)	Comments	Ref.
1.	**HPLC**	1×10^3	–	–	Expensive instrumentation, complicated column preparation, required sample pretreatment	[50]
2.	**Spectrophotometry**	8×10^3	$(8–2000)\times10^3$	81–116	Required sample pretreatment, interferences due to turbidity is not completely abolished	[51]
3.	**Flow injection analysis electrochemical determination**	3×10^2	$(6–13)\times10^2$	–	Expensive instrumentation, required sample pretreatment	[33]
4.	**Poly(methylene blue) modified electrode**	2×10^5	–	–	Sample pretreatment, complicated, and time consuming process of batch injection	[32]
5.	**Au electrode modified by self assembled monolayer of 2-mercaptodecylhydroquinone**	–	$(6–64)\times10^3$	–	No analysis in blood, no interferents studied	[34]
6.	**MIP-based electrochemical detection**	6.7	24.9–454.7	99–102	No sample pretreatment, easy handling and good for clinical analysis	This work

approximated to that of aqueous solution. As a matter of fact, the slope of calibration equation of blood sample studied was very close to that of the aqueous sample. As shown in Table 1, the sensor responded quantitative recoveries for all samples, and thus can be utilized as a practical sensor for clinical analysis. The proposed sensor for Hb is also compared with a known electrode (Poly (N-vinyl-2-pyrrolidone) (PVP)-capped CdS quantum dots (PCQDs) modified electrode) [33] by means of Student's *t-test* [t_{cal} (2.92) < t_{tab} (3.44), confidence limit 95%]. Although both methods are précised, the proposed sensor (*LOD* 6.80 ng mL^{-1}) is approximately 50 times more sensitive than the known method (*LOD* 322.50 ng mL^{-1}) of Hb sensing. The present method is also compared with other known methods utilized for Hb detection (Table 2). Accordingly, the proposed sensor is found to be best which requires no sample pretreatment and assures high selectivity and sensitivity for Hb analysis at trace level.

3.9. Cross-reactivity and sensor endurance

Influence of different interferents, viz., bovine serum albumin (BSA), tryptophan (Trp), C-reactive protein (Crp), glutamic acid (Glu), dopamine (Dop), Cys, ascorbic acid (AA), insulin (Ins), and their mixture on the determination of Hb was studied (Fig. S7, Supporting Information). Both MIP and NIP (before washing)-modified electrodes were not responsive for any interferents, when studied individually. A parallel cross-reactivity of binary mixtures of template and interferents(s) (taken in the clinically relevant concentration ratio, 1:10) was also explored (Fig. S7, Supporting Information). Despite quantitative results of Hb with MIP/QDs–MWCNTs/PGE, certain interferents like, Trp, Glu, Dop, Cys, AA, Ins and mixture of all interferents, taken in their clinically relevant concentration ratios with test analyte, have shown approximately 10% non-specific contributions on the NIP-modified PGE. However, such contributions could easily be curtailed simply by multiple water-washings (n=3, 0.20 mL). Therefore, as a safeguard to avoid any false-positive error, the MIP-modified sensor should also be subjected to similar washing treatment, before DPCSV measurement.

Stability and reproducibility of the proposed sensor were also examined. The sensor has shown long term stability (approximately 1 month) in terms of DPCSV response [For details vide Supporting Information (Section S9)].

4. Conclusion

For the first time, a MIP-based electrochemical sensor fabricated at the surface of QDs–MWCNTs nanoconjugate/PGE is reported for the determination of Hb in whole blood samples. The QDs-MWCNTs nanoconjugate has successfully been utilized for the surface imprinting in water that provided an excellent water-compatibility and biocompatibility to ensure high selectivity and sensitivity of the Hb measurement, without any denaturation and electrode passivation. This electrode can be recommended as a practical sensor for the Hb analysis at the stringent limits of highly diluted blood samples, since it requires no sample pretreatment, unlike other conventional spectrophotometric and high performance liquid chromatography (HPLC) analyses.

Acknowledgments

Authors thank Council of Scientific and Industrial Research–University Grant Commission (CSIR–UGC), New Delhi for granting a junior research fellowship to A.P. Instrumental facilities were procured out of a recent project (SR/S1/IC-30/2010) funded by the Department of Science and Technology, New Delhi.

Appendix A. Supporting information

Supplementary data associated with this article can be found in the online version at http://dx.doi.org/10.1016/j.talanta.2013.01.051.

References

[1] X.Q. Chen, Y. Zhou, X.J. Peng, J. Yoon, Chem. Soc. Rev. 39 (2010) 2120–2135.
[2] P.K. Sudeep, S.T.S. Joseph, K.G. Thomas, J. Am. Chem. Soc. 127 (2005) 6516–6517.
[3] C.A. Mirkin, R.L. Letsinger, R.C. Mucic, J.J. Storhoff, Nature 382 (1996) 607–609.
[4] M.Y. Han, X.H. Gao, J.Z. Su, S.M. Nie, Nat. Biotechnol. 19 (2001) 631–635.
[5] K. Zhang, H. Zhou, Q. Mei, S. Wang, G. Guan, R. Liu, J. Zhang, Z. Zhang, J. Am. Chem. Soc. 133 (2011) 8424–8427.
[6] U.H.F. Bunz, V.M. Rotello, Angew. Chem. Int. Ed. 49 (2010) 3268–3279.
[7] Q. Mei, Z. Zhang, Angew. Chem. Int. Ed. 51 (2012) 5602–5606.
[8] C. Chen, J. Peng, H.S. Xia, G.F. Yang, Q.S. Wu, L.D. Chen, L.B. Zeng, Z.L. Zhang, D.W. Pang, Y. Li, Biomaterials 30 (2009) 2912–2918.
[9] Y.J. Zhao, X.W. Zhao, B.C. Tang, W.Y. Xu, J. Li, J. Hu, Z.Z. Gu, Adv. Funct. Mater. 20 (2010) 976–982.
[10] R. Majithia, J. Patterson, S.E. Bondos, K.E. Meissner, Biomacromolecules 12 (2011) 3629–3637.
[11] A. Wolcott, D. Gerion, M. Visconte, J. Sun, A. Schwartzberg, S.W. Chen, J.Z.J. Zhang, Phys. Chem. B 110 (2006) 5779-578.
[12] J.K. Jaiswal, H. Mattoussi, J.M. Mauro, S.M. Simon, Nat. Biotechnol. 21 (2003) 47–51.
[13] J.K. Jaiswal, S.M. Simon, Trends Cell. Biol. 14 (2004) 497–504.
[14] Y. Tu, Q. Xu, Q-J. Zou, Z-H. Yin, Y-Y. Sun, Y-D. Zhao, Anal. Sci. 23 (2007) 1321–1324.
[15] Z-X. Cai, X-P. Yan, Nanotechnology 17 (2006) 4212–4216.
[16] J-L. Zhang, X-C. Tan, D-D. Zhao, S-W. Tan, Z-W. Huang, Y. Mi, Z-Y. Huang, Chem. Res. Chin. Univ. 26 (2010) 541–545.

[17] Z. Lu, W. Hu, H. Bao, Y. Qiaoab, C.M. Li, Med. Chem. Commun. 2 (2011) 283–286.
[18] N. Sinha, J. Ma, J.T.W. Yeow, J. Nanosci. Nanotechnol. 6 (2006) 573–590.
[19] Y. Zhao, Y. Ma, H. Li, L. Wang, Anal. Chem. 84 (2012) 386–395.
[20] S. Ge, C. Zhang, F. Yu, M. Yan, J. Yu, Sens. Actuators, B 156 (2011) 222–227.
[21] J. Liu, H. Chen, Z. Lin, J.M. Lin, Anal. Chem. 82 (2010) 7380–7386.
[22] M.H. Lee, Y.C. Chen, M.H. Ho, H.Y. Lin, Anal. Bioanal. Chem. 397 (2010) 1457–1466.
[23] C.I. Lin, A.K. Joseph, C.K. Chang, Y.D. Lee, Biosenors Bioelectron. 20 (2004) 127–131.
[24] C.I. Lin, A.K. Joseph, C.K. Chang, Y.D. Lee, J. Chromatogr. A 1027 (2007) 259–262.
[25] H.F. Wang, Y. He, J.R. Ji, X.P. Yan, Anal. Chem. 81 (2009) 1615–1621.
[26] H-T. Lian, B. Liu, Y-P. Chen, X-Y. Sun, Anal. Biochem. 426 (2012) 40–46.
[27] G. Guan, B. Liu, Z. Wang, Z. Zhang, Sensors 8 (2008) 8291–8320.
[28] J. Shi, D. Luo, Instrum. Sci. Technol. 33 (2005) 533–540.
[29] N. Kayoto, M. Hideko, K. Hajime, Anal. Biochem. 165 (1987) 28–32.
[30] Y.C. Zhu, G.J. Cheng, S. Dong, Biophys. Chem. 97 (2002) 129–138.
[31] A. Salimi, R. Hallaj, S. Soltanian, Biophys. Chem. 130 (2007) 122–131.
[32] C.M.A. Brett, G. Inzelt, V. Kertesz, Anal. Chim. Acta 385 (1999) 119–123.
[33] M. Liu, G. Shi, L. Zhang, Y. Cheng, L. Jin, Electrochem. Commun. 8 (2006) 305–310.
[34] J. Zhang, K. Seo, C. Jeon, Anal. Bioanal. Chem. 375 (2003) 539–543.
[35] R. Ouyang, J. Lei, H. Ju, Nanotechnology 21 (2010) 1–9 185502.
[36] Y. Wang, Z.H. Chai, H.Y. He, Y.Z. Jiang, G.Q. Fu, Chin. Chem. Lett. 21 (2010) 1487–1489.
[37] S. Wu, W. Tan, H. Xu, Analyst 135 (2010) 2523–2527.
[38] W. Lei, Z. Meng, W. Zhang, L. Zhang, M. Xue, W. Wang, Talanta 99 (2012) 966–971.
[39] P-P. Tang, J-B. Cai, Q-D. Su, Chin. J. Chem. Phys. 23 (2010) 195–200.
[40] B.M. Culbertson, M.H. Dotrong, Pure Appl. Chem. A 37 (2000) 419–431.
[41] B.B. Prasad, M.P. Tiwari, R. Madhuri, P.S. Sharma, J. Chromatogr. A 1217 (2010) 4255–4266.
[42] W. Gao, J. Song, J. Electroanal. Chem. 576 (2005) 1–7.
[43] A.M. Shanmugharaj, J.H. Bae, R.R. Nayak, S.H. Ryu, J. Polym., Sci. Part A: Polym. Chem. 45 (2007) 460–470.
[44] S.A. Piletsky, E.V. Piletskaya, T.L. Panasyuk, A.V. El'skaya, R. Levi, I. Karube, G. Wulff, Macromolecules 31 (1998) 2137–2140.
[45] D. Kriz, O. Ramstroem, K. Mosbach, Biotechnology 14 (1996) 163–170.
[46] D. Gao, Z. Zhang, M. Wu, C. Xie, G. Guan, D. Wang., J. Am. Chem. Soc. 129 (2007) 7859–7866.
[47] X.J. Han, W.M. Huang, J.B. Jia, Biosensors Bioelectron. 17 (2002) 741–746.
[48] E. Laviron, J. Electroanal. Chem. 101 (1979) 19–28.
[49] D.A. Skoog, F.T. Holler, T.A. Neiman, Principles of Instrumental Analysis, fifth ed., Harcourt Brace College Publishers, Orlando, 1998.
[50] M.E.D.C. Busto, M. Montes-Bayon, E. Anonb, A. Sanz-Medel, J. Anal. At. Spectrom. 23 (2008) 758–764.
[51] D.A. Noe, V. Weedn, W.R. Bell, Clin. Chem. 30 (1984) 627–630.